

1 **SPAM: Solar Spectrum Prediction for Applications and Modeling**

2 **Vera Nikolaeva^{1,2} and Evgeny Gordeev³**

3 ¹Arctic and Antarctic Research Institute, St. Petersburg, 199397 Russia.

4 ²Pushkov Institute of Terrestrial Magnetism, Ionosphere, and Radio Wave Propagation, Russian
5 Academy of Sciences, Moscow, 142191 Russia.

6 ³St. Petersburg State University, St. Petersburg, 199034 Russia.

7 Corresponding authors: Vera Nikolaeva (nikolaeva.vera@gmail.com) and Evgeny Gordeev
8 (evgeny.i.gordeev@spbu.ru)

9 **Key Points:**

- 10 • SPAM - empirical model of solar shortwave radiation at the top of the atmosphere,
11 parametrized by single ground-based F10.7 index.
- 12 • SPAM consists of two sub-models: Solar-SPAM for general use and Aero-SPAM for
13 aeronomy.
- 14 • SPAM is specially designed with the ability to make solar spectrum forecast, enabling to
15 monitor and forecast ionospheric photochemistry.

16 **Abstract**

17 Solar Spectrum Prediction for Applications and Modeling (SPAM) – a new empirical model of
18 solar X-Ray, EUV and FUV radiation flux at the top of the Earth’s atmosphere. The model is
19 based on 14 years of daily averaged TIMED spacecraft measurements from 2002 to 2016 when
20 the SEE sensors were regularly calibrated. We used a second-order parametrization of the
21 irradiance spectrum by a single parameter – the $F_{10.7}$ index, which is a reliable and consistently
22 observed measure of solar activity. The SPAM model consists of two submodels for general and
23 specific use. The first is the Solar-SPAM model of the photon energy flux in the first 190 nm
24 spectral bands, which can be used for a wide range of applications in different fields of research.
25 The second model, Aero-SPAM, is designed specifically for aeronomic research and provides a
26 photon flux for 37 specific wavelength intervals (20 wave bands and 16 separate spectral lines
27 within the range of 5–105 nm and an additional 121.5 nm Ly-alpha line), that play a major role
28 in the photoionization of atmospheric gas particles. We provide the full set of parameterization
29 coefficients that allows for immediate implementation of the model for research and
30 applications. In addition, we used the Aero-SPAM model to build a ready-to-use numerical
31 application for calculating the photoionization rates of the main atmospheric components N_2 , O_2 ,
32 O, N and NO with known absorption and ionization cross sections.

33 **Plain Language Summary**

34 The small part of the solar radiation spectrum in the range of 0–190 nm makes a decisive
35 contribution to the chemistry and dynamics of the Earth’s thermosphere and ionosphere,
36 becoming one of the governing parameters for space weather and global climate dynamics.
37 Variability of shortwave radiation flux in specific spectral ranges can exceed 50% during 27-day
38 solar rotation, order of magnitude in the course of the solar cycle, and several orders of
39 magnitude during solar flares. Solar radiation in this wavelength range is completely absorbed by
40 the upper atmosphere, providing a need for model development as an alternative to direct
41 satellite measurements. For the needs of space weather monitoring and forecasting, and many
42 other applications, we present the simple but accurate empirical model of the solar shortwave
43 radiation spectrum - SPAM (Solar Spectrum Prediction for Applications and Modeling),
44 parameterized by a single ground-based $F_{10.7}$ solar activity index. The model is based on 14 years
45 of spacecraft measurements and divided into two submodels: the Solar-SPAM model of the
46 photon energy flux in the wavelength range 0–190 nm, intended for general use, and the Aero-
47 SPAM model of photon flux in 37 specific wavelength intervals, intended to aeronomic
48 calculations.

49 **1 Introduction**

50 Operating at low Earth orbit, TIMED spacecraft provide measurements of the solar
51 radiation spectrum in the shortwave range 0–190 nm (Woodraska et al., 2004). Exactly this
52 radiation range is the main source of ion production at 80–200 km altitudes in the sunlit
53 atmosphere (e.g., Woods et al., 2000). The small part of the solar radiation spectrum from 0–190
54 nm, measured by the TIMED spacecraft, makes a decisive contribution to the chemistry and
55 dynamics of the Earth’s thermosphere and ionosphere (Lean et al., 2011; Vourlidas et al., 2018),
56 becoming one of the governing parameters for space weather (Lilensten et al., 2008) and global
57 climate dynamics including ozone variability (Rozanov et al., 2006; Gray et al., 2010; Fuller-
58 Rowell et al., 2004).

59 In the D-region and the lower part of the E-region of ionosphere the EUV band including
60 Ly-alpha continuum (centered on 121.5 nm) usually plays a major role in the photoionization
61 process with minor contributions from the X-ray (0–10 nm) and FUV (122–190 nm) irradiance.
62 However, during solar flares, the X-ray flux can increase by several orders of magnitude, which
63 leads to a significant increase in the photoionization of the D-region (Pacini and Raulin, 2006;
64 Kaufmann and Paes de Barros, 1969). The UV radiation from 100–190 nm induces the molecular
65 oxygen dissociation in mesosphere, contributing to the ozone layer formation (Brasseur and
66 Solomon, 2005). The EUV range of the radiation spectrum is absorbed by the upper atmosphere,
67 creating the ionosphere regular E and F1 layers (Chapman, 1931; Nusinov et al., 2000;
68 Nikolaeva et al., 2021b), which plays a crucial role in the propagation of HF radio waves
69 (Cervera et al., 2021; Gao et al., 2006).

70 Shortwave irradiance permanently changes together with changing Sun (solar cycle, solar
71 rotation, solar flares), which in turn leads to congruent variation of the chemical composition in
72 the upper atmosphere (Byram et al., 1956; Lean, 1987; Vaishnav et al., 2018; Ward et al., 2021;
73 Qian and Solomon, 2012; Svalgaard, 2013). Variability of shortwave radiation flux in specific
74 spectral ranges can exceed 50% during 27-day solar rotation, 200% in the course of the solar
75 cycle, and several orders of magnitude during solar flares (Lean et al., 2001).

76 Solar X-rays and UV irradiance is completely absorbed by the upper atmosphere, so
77 spacecraft measurements remain the only reliable source of information on the shortwave
78 radiation flux (Schmidtke, 2015; Kretzschmar et al., 2008; Del Zanna and Mason, 2018).
79 Spacecraft lifetime limits, their possible planned and unplanned outages, sensor degradation and
80 other reasons lead to the need of empirical modeling and spectrum reconstruction used for many
81 applications. This task is far from new, but given the strong variability of the shortwave
82 spectrum, the limited possibilities of its measurement and its strong influence on the chemistry of
83 the upper atmosphere, the problem of the solar spectrum modeling remains relevant (Tobiska,
84 1996; Woods, 2008; Lean, 1990; Tobiska and Eparvier, 1998).

85 There are a number of EUV models specially designed for atmospheric studies. The
86 publicly available EUVAC empirical model (Richards et al., 1994) is based on the Atmosphere
87 Explorer E spacecraft measurements from 1977 to 1981, and is widely used for aeronomy
88 research as a source of EUV radiation covering the wavelength range from 5 to 105 nm. The
89 model is parameterized by function $P_{10.7} = (F_{10.7A} + F_{10.7})/2$, where $F_{10.7}$ is the daily solar activity
90 index, and $F_{10.7A}$ is the 81-day average around the day of calculation. This formulation
91 significantly narrows the applicability of the model, making it impossible to use for the real-time
92 observations and forecasts. Moreover, (Nikolaeva et al., 2021a) revealed a significant systematic
93 deviation of the EUVAC results. The discrepancy between the simulated and measured total
94 EUV radiation is 20–40% depending on the solar activity level (Nikolaeva et al., 2022b).

95 With the launch of the TIMED spacecraft, the EUVAC model was further upgraded to
96 the HEUVAC version using measurements from 2003 to 2010, but its parametrization remained
97 the same as in EUVAC (Richards et al., 2006). However (Girazian and Withers, 2015) found that
98 during the solar minimum the HEUVAC soft X-ray irradiance is ~65% larger and Ly-alpha
99 continuum flux is ~30% smaller than spacecraft measurements. They suggested their own
100 model, but parameterized by the same function $P_{10.7}$, which again led to the inability of real-time
101 calculations and forecasts.

102 Flare irradiance spectral model (FISM) and the improved version FISM2 consider both
103 the quiet Sun variation and the solar flare component of irradiance spectrum (Chamberlin et al.,
104 2007; Chamberlin et al., 2008; Chamberlin et al., 2020). FISM is based on modification of the
105 solar minimum reference spectrum by summarizing irradiance variability from the solar cycle,
106 solar rotation and two solar flare components due to gradual and impulsive phase variations. All
107 contributions are modeled independently taking into account various proxies: $F_{10.7}$, MgII core-to-
108 wing ratio and Ly-alpha emission line, the 17.1 and 30.4 nm emission lines from SDO/EVE, as
109 well as the GOES X-ray radiation flux and its time derivative. FISM2 is currently available
110 through the LASP Interactive Solar Irradiance Data Center
111 (https://lasp.colorado.edu/lisird/data/fism_p_ssi_earth/), but the online version has a two-year
112 lag.

113 Nusinov et al. (2021) made a simple EUV and FUV spectrum model using TIMED
114 satellite data and parameterized by radiation flux in the Ly-alpha line. They propose to use their
115 model for the reconstruction of the shortwave radiation spectrum from the measurements of
116 spaceborne spectral-selective photometers with reduced spectral resolution.

117 The complexity of parameterization, model inaccessibility and unavailability of control
118 parameters in real time make it difficult to use solar irradiance models in aeronomic research and
119 especially in real-time monitoring and forecasting. For the needs of aeronomy and other
120 applications, we present the simple but accurate empirical model of the solar shortwave radiation
121 spectrum SPAM (Solar Spectrum Prediction for Applications and Modeling), parameterized by a
122 single ground-based $F_{10.7}$ solar activity index. The model is based on 14 years of TIMED
123 measurements and divided into two separate submodels: the Solar-SPAM model of the photon
124 energy flux spectrum for the wavelength range 0–190 nm with an initial TIMED resolution of 1
125 nm; and the Aero-SPAM model of photon flux in 37 wavelength intervals including 20 wave
126 bands and 16 separate spectral lines within the range of 5–105 nm with an additional Ly-alpha
127 line 121.5 nm, intended to aeronomic calculations.

128 **2 Data**

129 2.1 $F_{10.7}$ index

130 The solar activity index $F_{10.7}$ is the radio emission at 10.7 cm (2800 MHz) measured by
131 the ground-based receiver. The $F_{10.7}$ index has high correlation with sunspot numbers, ultraviolet
132 and visible solar irradiance that make it an excellent measure of solar activity. The $F_{10.7}$
133 observational series is one of the longest among solar activity indices. Everyday measurements
134 have been publicly available since 1947 (Tapping, 2013). Also, the reliable forecast of the $F_{10.7}$
135 index (Gaidash et al. 2017; Huang et al., 2009; Lei et al., 2019; Henney et al., 2012; Zhang et al.,
136 2022) gives an opportunity to predict the upper atmosphere state up to 55 days.

137 In this study the daily solar $F_{10.7}$ index was taken from the OMNI database
138 (<https://omniweb.gsfc.nasa.gov/ow.html>). The $F_{10.7}$ index traditionally measures in solar flux
139 units (s.f.u.), one s.f.u. equals $10^{-22} \text{ W}\cdot\text{m}^{-2}\cdot\text{Hz}^{-1}$.

140 2.2 TIMED spacecraft data

141 The TIMED spacecraft (Thermosphere Ionosphere Mesosphere Energetics and
142 Dynamics) was commissioned on December 7, 2001 and is still in operation. One of the

143 scientific objectives of the TIMED mission is to study the mesosphere and lower thermosphere
144 dynamics under the influence of solar shortwave irradiance.

145 The SEE device (Solar EUV Experiment) (Woodraska et al., 2004) was developed for the
146 TIMED mission at the University of Colorado. The SEE data represent the solar spectrum from 0
147 to 190 nm covering X-ray (0–10 nm), EUV (10–122 nm) and FUV (122–190 nm) spectrum
148 ranges with 1 nm spectral and 97-minute temporal resolution. The SEE device observes the Sun
149 for about 3 minutes on each orbit, which gives 14–15 measurements per day. The SEE data is
150 then processed to Level 3A by applying correction for atmospheric absorption and sensor
151 degradation and averaging over each 3-minute observational interval. Here we use the Level 3A
152 SEE data (<http://lasp.colorado.edu/home/see/data>) to develop the empirical model of solar
153 shortwave irradiance SPAM.

154 The SEE data represents the total energy flux in each 1 nm wide spectral interval. In the
155 following, we will use the center point to define a specific interval, e.g., speaking of the spectral
156 channel 11.5 nm, we mean the same as the spectral band 11–12 nm.

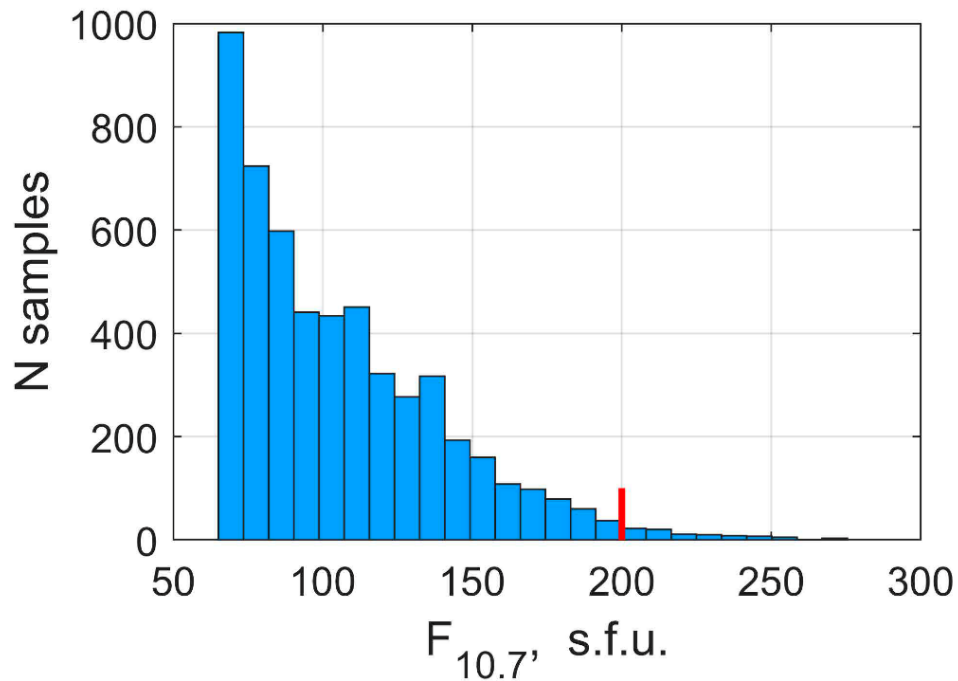
157 Several sounding rocket launches were undertaken during the mission to detect
158 degradation trends and calibrate the SEE detector. The last suborbital calibration flight was
159 carried out on June 1, 2016. Analyzing the spacecraft data, we found suspicious behavior of the
160 radiation flux in some of the SEE spectral channels beginning from December 2016, soon after
161 the last sensor calibration (more details in the Discussion section). Although the TIMED
162 spacecraft is still in operation, we limit the SEE data used in development of the SPAM model to
163 the interval from 22.01.2002 to 24.11.2016.

164 **3 Solar-SPAM: shortwave energy spectrum model**

165 The model is based on the long time series of X-Ray, EUV and FUV solar irradiance
166 received by the TIMED SEE instrument from 22.01.2002 to 24.11.2016. The histogram in Figure
167 1 shows the distribution of 5368 daily averaged spectra samples against the SPAM control
168 parameter $F_{10.7}$. Since the number of samples clearly decreases with increasing solar activity, we
169 set the limits on the data used in the SPAM model development to $65 < F_{10.7} < 200$ s.f.u., which
170 includes 95% of all measured data. These limits can also be considered as the limits of
171 applicability of the model.

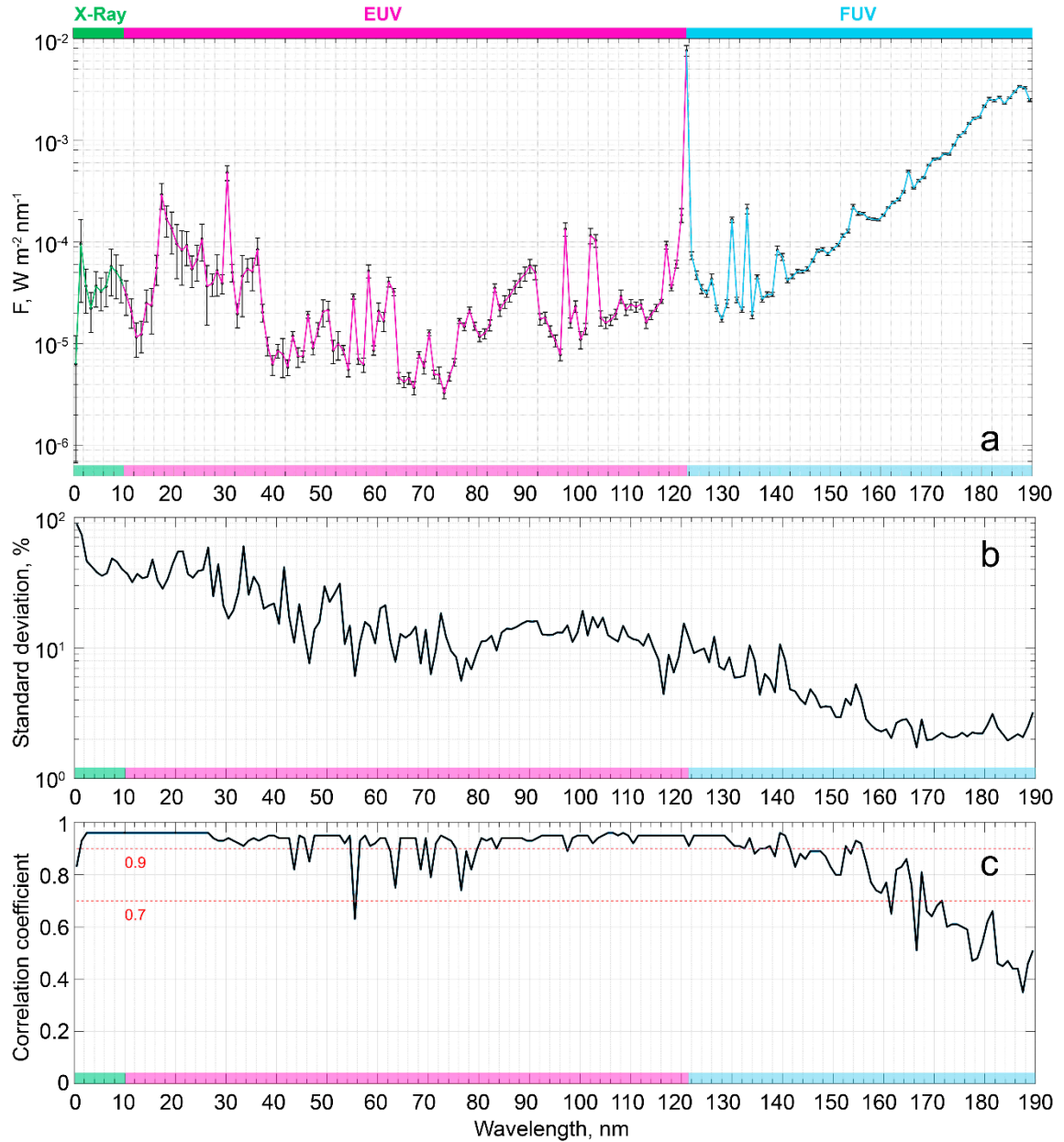
172 Figure 2a shows the average energy spectrum based on TIMED measurements from 2002
173 to 2016. The vertical bars denote the standard deviation in each spectral channel from 0 to 190
174 nm. The average spectrum has a complex structure with sharp changes in the energy flux by an
175 order of magnitude even in neighboring channels.

176



177
 178 **Figure 1.** Distribution of TIMED data, used to develop the SPAM model against F10.7 solar
 179 activity index.
 180

181 It is worth noting how strongly the level of variability changes with increasing
 182 wavelength. If the values of the X-ray energy flux vary more than an order of magnitude, then
 183 for the EUV range the energy flux changes only several times, and even less changes at the edge
 184 of the measured FUV range — within a few tens of percent (see examples in Figure 3 and
 185 Supplementary Material for the full set of scatterplots). To illustrate the level of irradiance
 186 variability more specifically, we show the relative standard deviation of the measured energy
 187 flux as a function of wavelength (Figure 2b). The standard deviation value drops exponentially
 188 from 100% to 2% with increasing wavelength from 0 to 190 nm.
 189



190
 191 **Figure 2.** Panel a: Average energy spectrum in the range of 0–190 nm built on the TIMED SEE
 192 data. Standard deviation is shown as a vertical line in each 1 nm wide spectral channel; Panel b:
 193 Relative standard deviation, note the logarithmic scale; Panel c: correlation coefficient.
 194

195 The naturally low variability of the FUV energy flux (Figure 3) in the course of the solar
 196 cycle leads also to low correlation coefficients in the spectral interval from 170 to 190 nm. The
 197 distribution of correlation coefficients over wavelengths is shown in Figure 2c. Most of the
 198 spectral bands demonstrate a high accuracy of the fitting procedure, and the value of the
 199 correlation coefficient exceed 0.7 for most and 0.9 for many spectral bands.

200 Continuous TIMED observation time series makes it possible to obtain a reliable
 201 functional dependence between the differential energy flux and solar activity index $F_{10.7}$. The
 202 second order polynomial suggested as a best fit function by (Bruevich and Yakunina, 2019) for

203 parameterization of the flux intensity in separate spectral lines of HeII (30.4 nm), HeI (58.4 nm),
204 CIII (97.8 nm) and FeXVIII (9.4 nm) in 24-th cycle by $F_{10.7}$ index. As a result of data analysis,
205 we found that the second-order parameterization is also valid for the entire shortwave radiation
206 spectrum measured by TIMED spacecraft, including X-Ray, EUV and FUV radiation. Thus,
207 when developing the Solar-SPAM model, we used the parametrization of the energy flux F in
208 each individual SEE spectral channel in the following form:

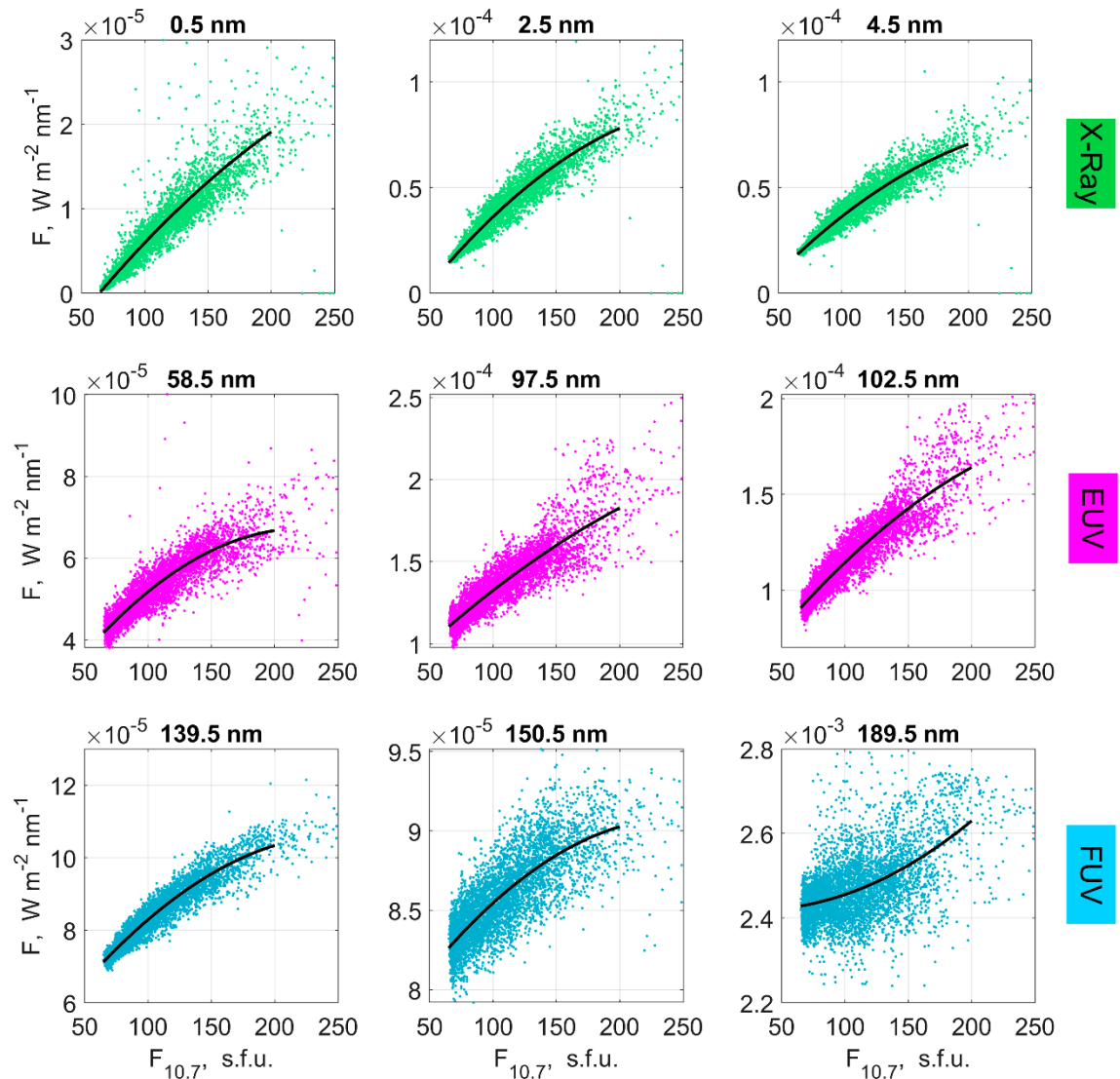
$$209 \quad F = P_1 \cdot F_{10.7}^2 + P_2 \cdot F_{10.7} + P_3, \quad (1)$$

210 where P_1 , P_2 and P_3 are regression coefficients, $F_{10.7}$ is a daily averaged value of the
211 index.

212 Figure 3 shows the scatterplots of energy flux measurements as a function of $F_{10.7}$ index
213 and their quadratic fitting functions for several X-Ray, EUV and FUV spectral channels: 0.5, 2.5,
214 4.5, 58.5 (contains HeI 58.4 nm line), 97.5 (contains CIII 97.8 nm line), 102.5 (contains Ly-beta
215 102.6 nm line), 139.5, 150.5 and 189.5 nm.

216 The entire set of regression coefficients of the Solar-SPAM model (Eq. 1) is collected in
217 Table A1 in Appendix A and can be instantly applied to reconstruct the model of the solar
218 radiation spectrum. Table A1 also includes the correlation coefficients (R) and root mean square
219 errors (RMSE) to demonstrate the level of confidence of the Solar-SPAM model.

220 The high variability of the shortwave solar radiation, especially in the X-ray and EUV
221 range, naturally provides a wide range of possible ionospheric and thermospheric conditions and
222 should be taken into account in aeronomic modeling and research. The next section is devoted to
223 the development of a specific model intended for aeronomic studies.



224
225
226
227

Figure 3. The scatterplots of TIMED energy flux measurements F versus $F_{10.7}$ index for 0.5, 2.5, 4.5, 58.5, 97.5, 102.5, 139.5, 150.5, 189.5 nm. Black lines are the second order polynomial fitting functions.

228 **4 Aero-SPAM: EUV photon flux model for aeronomic applications**

229 Here we present the development of an empirical model of solar irradiance suitable for
230 aeronomic studies, as well as its ready-to-use application for calculating photoionization rates in
231 the vertical column of the atmosphere. There is a set of well-defined spectral bands and
232 individual spectral lines responsible for the photoionization of the main atmospheric neutrals
233 with known absorption and ionization cross sections (Torr and Torr, 1979; Banks and Kockarts,
234 1973; Ohshio et al., 1966). According to this set, we have reduced the TIMED data to 20 spectral
235 intervals from 5 to 105 nm with a width of 5 nm each and 16 individual spectral lines, in
236 correspondence to the EUVAC model (Richards et al., 1994). Additionally, we included to our
237 model the strong spectral line Ly-alpha ($\lambda = 121.5$ nm) which is responsible for the nitric oxide
238 ionization in the lower ionosphere. The radiation flux in each 5 nm interval is calculated by

239 direct summation of the flux in the SEE channels that fall into this interval, while the flux in an
 240 individual spectral line is assumed to be equal to the flux in the corresponding 1 nm wide SEE
 241 channel.

242 For aeronomic applications, such as the calculation of photoionization rate in the upper
 243 atmosphere, solar irradiance is usually expressed in units of photon flux. Therefore, we
 244 converted the differential energy flux (F , $\text{W}\cdot\text{m}^{-2}\cdot\text{nm}^{-1}$) measured by TIMED SEE device into a
 245 differential photon flux (I , $\text{m}^{-2}\cdot\text{s}^{-1}\cdot\text{nm}^{-1}$) by dividing the original flux by the photon energy,
 246 corresponding to each spectral channel: $I = F/(hc/\lambda)$, where h – is Planck's constant, c – is the
 247 speed of light, and λ – is the central wavelength of each 1-nm SEE channel.

248 Further development of the model is fully consistent with the procedure used in the
 249 previous chapter. We use daily averaged data and a second-order polynomial fit to formulate the
 250 Aero-SPAM model:

$$251 \quad I = P_1 \cdot F_{10.7}^2 + P_2 \cdot F_{10.7} + P_3, \quad (2)$$

252 where P_1 , P_2 and P_3 are regression coefficients, $F_{10.7}$ is a daily averaged value of the
 253 index. The photon flux I is calculated in 20 spectral intervals and 17 individual spectral lines
 254 listed in Table A2 in Appendix A, together with model coefficients, R and RMSE values.

255 Photoionization of the atmosphere by solar EUV is a main source of the regular
 256 ionospheric layers E and F_1 formation. The Aero-SPAM model is specifically developed for the
 257 calculation of photoionization rates in the Earth's upper atmosphere and can be used in many
 258 aeronomic applications and research. As an example, it is already integrated into the AIM-E
 259 numerical model of the ionosphere (Nikolaeva et al., 2021b; Nikolaeva et al., 2022a) as a part of
 260 the photoionization module. Below we provide a description, as well as a ready-to-use numerical
 261 module for calculating the photoionization rates of atmospheric gases using the Aero-SPAM
 262 model.

263 The photoionization rate $q_j(z)$ of the neutral gas j -th component at the altitude z is the
 264 number of photoionization acts per unit volume per unit time. Here we determine the
 265 photoionization rates for N, O, NO, N_2 and O_2 using expression (Shunk and Nagy, 1980):

$$266 \quad q_j(z) = n_j \sum_{\lambda} \sigma_{j\lambda}^i I_{\lambda}^{\infty} \exp\left(-\sum_n \sigma_{n\lambda}^a \int_z^{\infty} \text{Ch}(\chi) n_n dz\right), \quad (3)$$

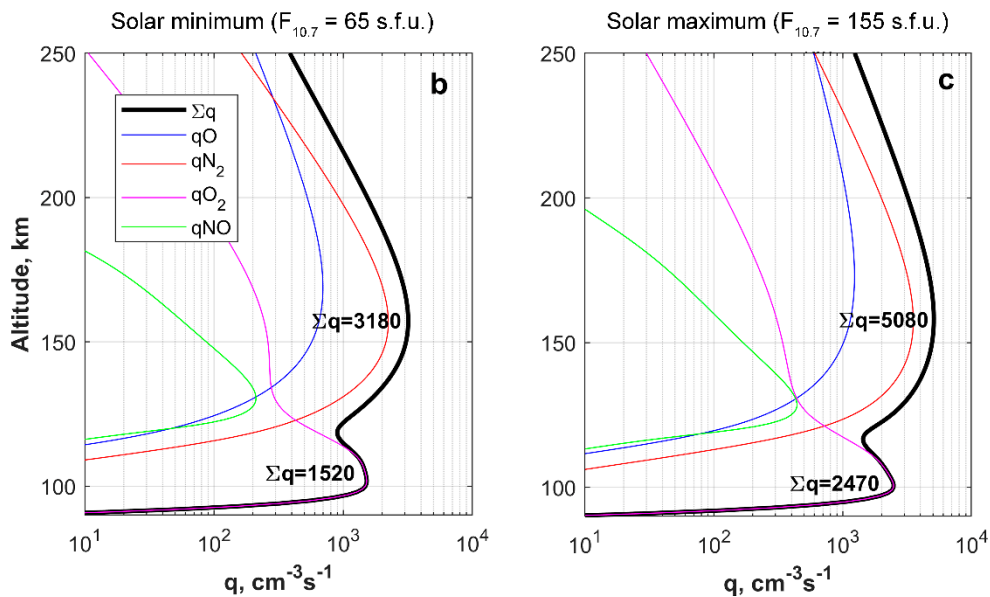
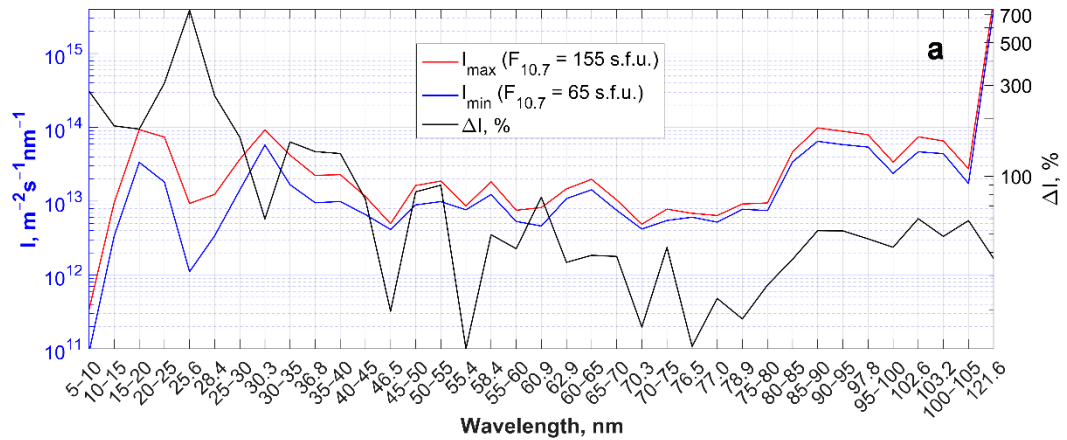
267 where n_j – concentration of the j -th component of atmospheric gas, $\sigma_{j\lambda}^i$ – its
 268 photoionization cross section at wavelength λ , $\sigma_{j\lambda}^a$ – its photoabsorption cross section at
 269 wavelength λ , $\text{Ch}(\chi)$ – the extended Chapman function (Chapman, 1931; Smith and Smith, 1972)
 270 and I_{λ}^{∞} – photon flux at wavelength λ at the top of the atmosphere, provided by Aero-SPAM
 271 model.

272 To illustrate the aeronomic application of the Aero-SPAM model we reconstruct the solar
 273 irradiance spectrum and calculate the vertical profiles of the photoionization rates (Eq. 3) during
 274 solar activity minimum 2009 June 20, and maximum 2015 June 18 (Fig. 4). The neutral
 275 atmosphere composition and temperature, required for the calculations, were taken from the
 276 NRLMSISE-00 model (Picone et al., 2002) hosted at the Community Coordinated Modeling
 277 Center (<https://ccmc.gsfc.nasa.gov/>), while the nitric oxide density, which is not represented in
 278 the MSISE model, was obtained from the E Region Auroral Ionosphere Model (AIM-E)
 279 (Nikolaeva et al., 2021b).

280 The values of $F_{10.7}$ solar activity index for the selected days 2009 June 20 and 2015 June
281 18 are 65 s.f.u. and 155 s.f.u., correspondingly. The differential photon flux changes significantly
282 between minimum and maximum of the solar cycle (Fig. 4a). It is worth noting that the ratio of
283 variation is not the same for different bands and spectral lines. For example, as it shown in
284 Figure 4a, the change of the photon flux in the 25.6 nm line $\Delta I_{25.6} \sim 700\%$, whereas in the Ly-
285 alpha line $\Delta I_{121.6} \sim 50\%$. Such a notable change in the spectrum of solar radiation leads to
286 significant changes in atmospheric photochemistry and in the overall dynamics of the
287 ionosphere.

288 Figure 4 (b, c) shows the vertical distribution of photoionization rates q between 90 and
289 250 km above the subauroral station Gorkovskaya (60.27°N, 29.38°E) at 12h MLT for the
290 molecular oxygen and nitrogen (O_2 and N_2), atomic oxygen (O) and nitric oxide (NO). The
291 altitude distribution of the total photoionization rate has two peaks at ~ 100 km and ~ 160 km. The
292 first peak (~ 100 km) of the photoionization rate leads to the formation of the ionospheric regular
293 layer E approximately in the same altitudes. The photoionization here is totally dominated by
294 qO_2 , and changes more than 50% in the course of the solar activity cycle. The second peak
295 (~ 160 km) of the photoionization rate is one of the main sources of formation of the regular layer
296 F_1 , together with the vertical plasma drift. It is formed mainly due to the qN_2 component which
297 differs by about 70% for the minimum and maximum of the considered solar cycle. While the
298 qNO value is several times lower than the photoionization rates of other components, the
299 difference between the qNO profiles shown in Fig. 4 (b, c) is huge: $\sim 250\%$ for the E layer
300 heights and $\sim 400\%$ for the F layer heights. Despite the low photoionization rate, qNO has a
301 significant effect on the electron concentration in the ionosphere due to the relatively high
302 density of neutral NO content in the upper atmosphere.

303 For the chemical models of the ionosphere (e.g., Verronen et al., 2016; Nikolaeva et al.,
304 2021b; Lanchester et al, 2001), it is extremely important to take into account the changes in the
305 shape of the solar radiation spectrum and the corresponding change in the vertical distribution of
306 photoionization rates. Our Solar-SPAM and Aero-SPAM models accurately track these changes
307 over the course of the changing Sun. Both models, as well as the photoionization rate module,
308 are available on GitHub as ready-to-use Matlab scripts (<https://github.com/magnetophys/SPAM>).



309
 310 **Figure 4.** Panel **a**: simulated differential photon flux using Aero-SPAM model during the solar
 311 activity minimum at 2009 June 20 (blue line) and during solar activity maximum at 2015 June 18
 312 (red line) and their relative difference (black line). Panels **b** and **c**: vertical distribution of the
 313 photoionization rates between 90 and 250 km above the Gorkovskaya station (60.27°N, 29.38°E)
 314 during the minimum and maximum of the solar activity cycle. The calculations were carried out
 315 for the photoionization rates of molecular oxygen O₂ (magenta), molecular nitrogen N₂ (red),
 316 atomic oxygen O (blue), nitric oxide NO (green) and total ionization rate (black) for the local
 317 noon during summer solstices.

318 5 Discussion

319 One of the main requirements for building a good empirical model is the reliability of the
 320 measurements, which becomes especially important in case of solar shortwave irradiance. The
 321 point is that the Earth's atmosphere completely absorbs solar irradiance in the range 0–190 nm,
 322 so measurements can only be carried out on board the spacecraft, which makes it difficult to
 323 continuously control the quality of received data. The sensitivity of the photosensors may suffer
 324 during prolonged operation of instruments in space, leading to systematic errors and false trends

325 in observations (Dudok de Wit, 2022). To build an accurate model, it is necessary to exclude
326 data distorted due to sensor degradation.

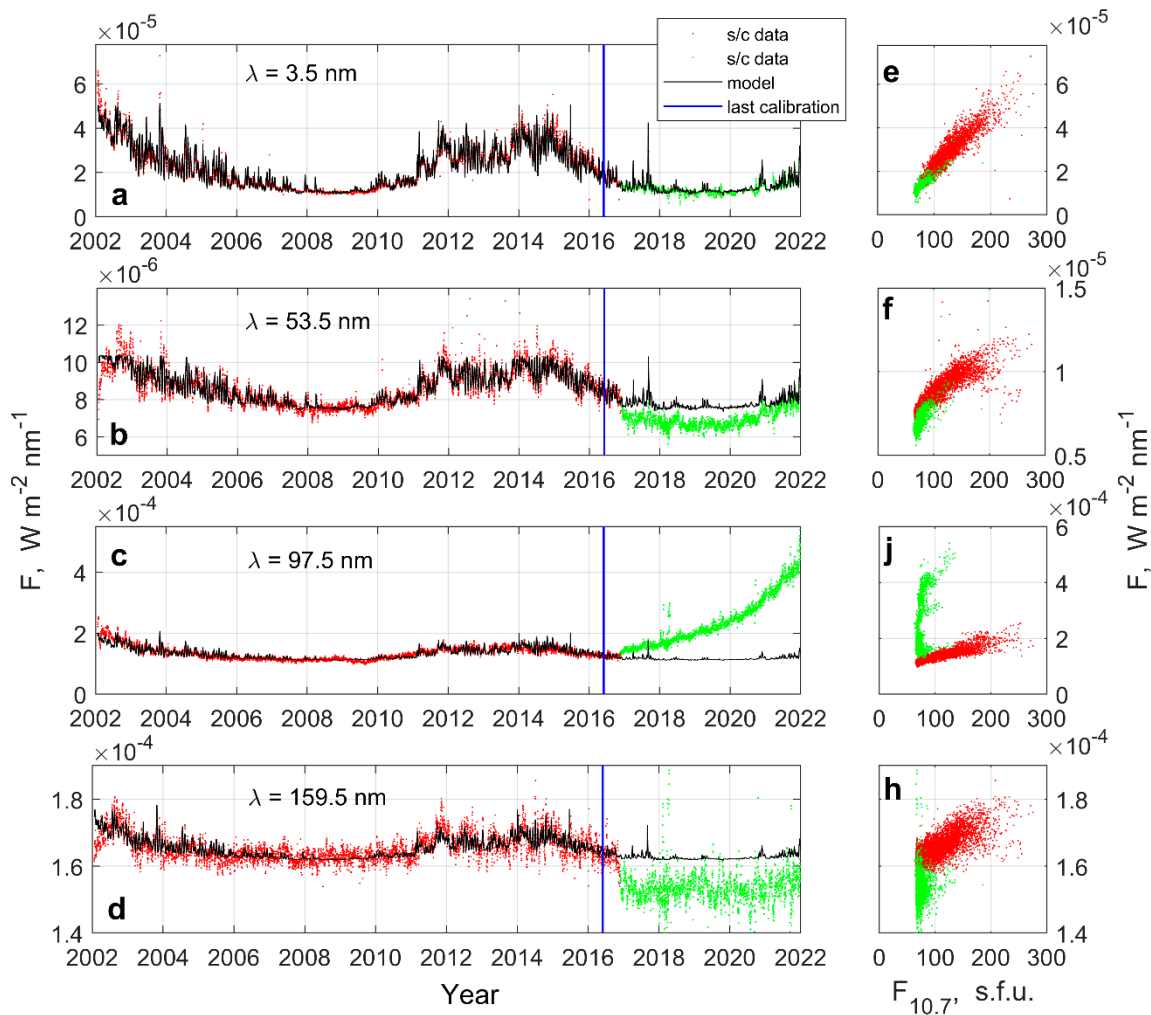
327 One of the few ways to calibrate instruments onboard a spacecraft (e.g. Mauceri et al.,
328 2020; Snow et al, 2010; Klimov et al., 2021) is to launch a sounding rocket (e.g., Didkovsky et
329 al., 2009) with a copy of the instrument on board. This method was used for calibration of the
330 TIMED SEE device.

331 There were nine SEE suborbital calibration flights during 2002–2013 years, and after
332 them the last one was launched on June 1, 2016
333 (http://lasp.colorado.edu/data/timed_see/level3a/README_SEE_L3A_012.TXT). Thus, the
334 TIMED SEE data from 2002 to 2016 can be considered well calibrated and reliable for model
335 development.

336 We noticed non-typical trends in spacecraft measurements made after the last calibration
337 rocket launch in 2016, apparently related to the SEE detector degradation, that are not indicated
338 in the “Known Issues/Problems” section of the actual instrument’s release notes
339 (http://lasp.colorado.edu/data/timed_see/SEE_v12_releasenotes.txt).

340 Figure 5 shows several examples of the solar irradiance time series in different spectral
341 lines. Panels a–d demonstrate the TIMED SEE measurements (red and green) for the entire
342 period of spacecraft operation from 2002 to 2022 years, divided by the vertical blue line that
343 denotes the date of the last calibration launch of a suborbital rocket on June 1, 2016. Half a year
344 after the last calibration, artificial trends appeared in different spectral lines, which are easy to
345 recognize by the abrupt shift in the measured values. Data obtained before sensor degradation is
346 shown in red, and after – in green. The black curve denotes the Solar-SPAM calculations based
347 on the daily averaged $F_{10.7}$ index.

348 Examples in Figure 5 demonstrate that different spectral lines of the detector were
349 affected to varying degrees. Thus, for the 3.5 nm line (Fig. 5a) there is no visible jump in the
350 measured radiation flux and there is a good agreement between the data and model calculations.
351 This is generally true for the first 27 SEE channels covering the 0–28 nm spectral range. The
352 situation changes dramatically in the case of all other SEE channels. For example, the sharp drop
353 in the radiation flux can be seen in 53.5 and 159.5 nm lines shortly after the last calibration in
354 2016 (Fig. 5 b and d). At the same time, there is an unusual growth in the 97.5 nm line (more
355 than 200% in comparison with the previous solar cycle) throughout the following years. We
356 conclude the presence of anomaly in the TIMED SEE data after last calibration in 2016, which is
357 not associated with the solar activity variations.



358
 359 **Figure 5.** Solar irradiance time series in different spectral lines: **a** – 3.5 nm; **b** – 53.5 nm; **c** –
 360 97.5 nm; **d** – 159.5 nm. TIMED SEE measurements shown in red (before) and in green (after
 361 sensor degradation); black curve is the Solar-SPAM calculations. Blue vertical line denotes the
 362 date of the last absolute detector calibration on June 1, 2016. Panels **e–h** show scatterplots of the
 363 radiation flux versus the F10.7 solar activity index.

364 All measurement time series for each individual SEE channel can be found in
 365 Supplementary Materials 1 in the same format as in Fig. 5.

366 6 Conclusions

367 SPAM – an empirical model for the solar irradiance spectrum has been developed using
 368 14 years of TIMED spacecraft observations from 2002 to 2016. The model covers the X-Ray (0–
 369 10 nm), EUV (10–122 nm) and FUV (122–190 nm) spectral intervals with 1 nm resolution. The
 370 model is parametrized by single $F_{10.7}$ index – the solar radio flux at 10.7 cm, that gives a number
 371 of advantages:

372 1) The $F_{10.7}$ index is an excellent indicator of solar activity (Tapping, 2013) and may
 373 serve as a reliable proxy for the solar spectrum variations within the limits of the SPAM model
 374 applicability $65 < F_{10.7} < 200$ s.f.u.

375 2) Since the atmosphere is transparent to radiation at a wavelength of 10.7 cm, the $F_{10.7}$
 376 radio flux can be reliably measured from the Earth's surface in any weather. The time series of
 377 the daily $F_{10.7}$ has been available continuously since 1947 for seven solar cycles, so the SPAM
 378 model can be applied for a large-time-scale climatology studies requiring the solar irradiance
 379 variations.

380 3) The $F_{10.7}$ index is predictable, which allows SPAM to forecast the solar spectrum for
 381 various operational tasks. There are a number of services providing the forecast of the daily-
 382 averaged $F_{10.7}$ index, e.g., up to 55 days ahead
 383 (<http://spaceweather.izmiran.ru/eng/forecasts.html>), up to 27 days ahead open access forecast
 384 (<https://www.swpc.noaa.gov/products/27-day-outlook-107-cm-radio-flux-and-geomagnetic-indices>), up to 45 days ahead with 5-day resolution (<https://www.swpc.noaa.gov/products/usaf-45-day-ap-and-f107cm-flux-forecast>). Also, there is a long-term monthly average $F_{10.7}$ forecast
 386 up to 20 years including the next solar activity cycle that can be used for the future climate
 387 estimations (<https://www.swpc.noaa.gov/products/predicted-sunspot-number-and-radio-flux>).

389 4) The SPAM's single-variable parameterization is easy to implement. Despite the model
 390 simplicity, our results are in a good agreement with measurements.

391 Special part of the study is given to the aeronomy-oriented model Aero-SPAM. It
 392 provides photon flux values in 17 spectral lines and 20 bands, covering the 5–105 nm EUV range
 393 and additionally including the Ly-alpha 121.5 nm spectral line which is the main source of NO^+
 394 formation. The Aero-SPAM model is used to calculate the ionization rates of the neutral
 395 atmosphere gasses (N_2 , O_2 , O , N and NO) with well-known absorption and ionization cross
 396 sections. The Aero-SPAM model for aeronomy calculations can be applied to monitor and
 397 forecast ionospheric regular E and F_1 regions.

398 Acknowledgments

399 SPAM development and results analysis was supported by the Russian Science
 400 Foundation grant 20-72-10023. Software development was carried out within the framework of
 401 Russian Science Foundation grant 19-77-10016. SPAM application for the upper atmosphere
 402 was supported by the Ministry of Science and Higher Education of the Russian Federation under
 403 agreement 075-15-2021-583.

404 APPENDIX A

405 **Table A1:** The Solar-SPAM model describing the solar irradiance spectrum (F , $\text{W}\cdot\text{m}^{-2}\cdot\text{nm}^{-1}$)
 406 depending on the daily $F_{10.7}$ index, $F = P_1 \cdot F_{10.7}^2 + P_2 \cdot F_{10.7} + P_3$. P_1 , P_2 and P_3 are the regression
 407 coefficients for the X-Ray, EUV and FUV spectral intervals (λ) with 1 nm resolution. R is a
 408 correlation coefficient between $F_{10.7}$ index and measured photon energy flux, RMSE – root-
 409 mean-square error calculated for each wavelength λ .
 411

λ , nm	P_1	P_2	P_3	R	RMSE
0.5	$-2.58825263\text{e-}10$	$2.09144982\text{e-}07$	$-1.23612166\text{e-}05$	0.83	$3.14245291\text{e-}06$
1.5	$-4.94024181\text{e-}09$	$3.22175699\text{e-}06$	$-1.80553335\text{e-}04$	0.93	$2.67305197\text{e-}05$
2.5	$-1.51234762\text{e-}09$	$8.72873177\text{e-}07$	$-3.59300652\text{e-}05$	0.96	$4.64649582\text{e-}06$

3.5	-8.19051896e-10	4.76131943e-07	-1.75069528e-05	0.96	2.57208191e-06
4.5	-1.25299002e-09	7.18966612e-07	-2.30913459e-05	0.96	3.78321360e-06
5.5	-1.05306909e-09	6.00386365e-07	-1.72945105e-05	0.96	3.13381799e-06
6.5	-1.24449248e-09	7.07626722e-07	-2.22302072e-05	0.96	3.69094684e-06
7.5	-2.59694610e-09	1.45374662e-06	-6.31698909e-05	0.96	7.43469515e-06
8.5	-2.16866639e-09	1.21455389e-06	-4.96505577e-05	0.96	6.21501074e-06
9.5	-1.52361462e-09	8.68533191e-07	-3.02456892e-05	0.96	4.53196359e-06
10.5	-1.01521500e-09	5.78430109e-07	-1.79161041e-05	0.96	3.02874105e-06
11.5	-5.92986152e-10	3.39846459e-07	-7.46323908e-06	0.96	1.86757596e-06
12.5	-3.91620799e-10	2.22633150e-07	-6.85281881e-06	0.96	1.16787269e-06
13.5	-3.68662392e-10	2.14384736e-07	-5.53046688e-06	0.96	1.20433914e-06
14.5	-8.15473279e-10	4.56904530e-07	-1.28641555e-05	0.96	2.34443139e-06
15.5	-1.05314223e-09	5.90337830e-07	-2.51992115e-05	0.96	3.02143819e-06
16.5	-1.71833912e-09	9.58528730e-07	-2.37694140e-05	0.96	4.91384954e-06
17.5	-7.84248508e-09	4.35156360e-06	-6.77832612e-05	0.96	2.24071577e-05
18.5	-5.35989584e-09	2.98171616e-06	-7.78638812e-05	0.96	1.53019138e-05
19.5	-5.64009182e-09	3.15119971e-06	-1.24435988e-04	0.96	1.61351843e-05
20.5	-4.90601610e-09	2.74377445e-06	-1.31174042e-04	0.96	1.40380060e-05
21.5	-4.26086127e-09	2.38514084e-06	-1.14409417e-04	0.96	1.22091037e-05
22.5	-3.19159017e-09	1.77982999e-06	-5.49342607e-05	0.96	9.12119600e-06
23.5	-1.75266637e-09	9.77475268e-07	-2.67796958e-05	0.96	5.01372608e-06
24.5	-2.43810818e-09	1.36192347e-06	-4.57043670e-05	0.96	6.97290978e-06
25.5	-3.98387625e-09	2.22551933e-06	-7.70072803e-05	0.96	1.13958300e-05
26.5	-2.00773403e-09	1.12849376e-06	-5.67602506e-05	0.96	5.77108499e-06
27.5	-1.19730867e-09	5.65394676e-07	-5.85964757e-06	0.94	3.19981683e-06
28.5	-1.46295195e-09	1.01404261e-06	-3.58365291e-05	0.93	8.68678105e-06
29.5	-8.15084563e-10	4.34467210e-07	3.65433670e-06	0.93	3.03848274e-06
30.5	-7.05077152e-09	4.04741769e-06	1.43586031e-04	0.94	2.75155631e-05
31.5	-7.77266741e-10	4.68802536e-07	1.08074811e-05	0.93	3.64885891e-06
32.5	-5.61602010e-10	2.83431306e-07	-3.27491491e-06	0.92	2.03502960e-06
33.5	6.11880133e-10	6.52060422e-07	-2.90103367e-05	0.91	1.14428500e-05
34.5	-2.13887412e-09	9.00810935e-07	-1.41575668e-05	0.93	5.08999204e-06
35.5	-2.29655541e-09	1.06445240e-06	-3.23960927e-05	0.94	6.31089521e-06
36.5	-1.69356060e-09	1.14642019e-06	-1.49427472e-05	0.93	9.15296502e-06
37.5	-4.44754965e-10	2.24144087e-07	2.29852502e-06	0.94	1.39955751e-06
38.5	-2.57264554e-10	1.20451838e-07	1.08315857e-07	0.95	6.47189724e-07
39.5	-1.90799471e-10	8.54129718e-08	-3.66570920e-07	0.95	4.29404481e-07
40.5	-1.63110170e-10	7.67917532e-08	2.48479107e-06	0.94	4.43317217e-07
41.5	-2.64676272e-10	1.61050402e-07	-5.64014188e-06	0.94	1.09306430e-06
42.5	-8.80727378e-11	5.09406819e-08	1.64104876e-06	0.94	3.40898878e-07
43.5	-1.29810569e-11	3.70763160e-08	8.20072441e-06	0.82	7.51972352e-07
44.5	-1.92736419e-10	9.35286333e-08	2.78944317e-08	0.95	5.03560346e-07
45.5	-1.07354187e-10	5.33853880e-08	3.23226206e-06	0.94	3.25167635e-07
46.5	7.14925370e-11	2.28505089e-08	1.60620921e-05	0.85	7.85818717e-07
47.5	-1.65354143e-10	7.61012429e-08	3.10560608e-06	0.95	3.96736808e-07
48.5	-3.12973348e-10	1.39150026e-07	3.17305408e-06	0.95	6.77782659e-07
49.5	-8.48676578e-10	3.82780831e-07	-8.99955570e-06	0.95	1.84750385e-06
50.5	-6.92148698e-10	3.05273387e-07	-2.21022224e-06	0.95	1.42588987e-06
51.5	-3.52451773e-10	1.49567940e-07	-2.77810793e-06	0.95	6.67205223e-07
52.5	-4.88285423e-10	2.06597500e-07	-5.71616451e-06	0.95	9.23676788e-07
53.5	-1.51950475e-10	6.22135728e-08	4.00946070e-06	0.92	3.69972956e-07
54.5	-1.47270077e-10	5.88009296e-08	1.18884773e-06	0.95	2.61720547e-07
55.5	-2.67639507e-10	9.72464276e-08	2.22162082e-05	0.63	1.37799232e-06

56.5	-1.01960607e-10	4.67610258e-08	3.41494514e-06	0.93	2.80937628e-07
57.5	-1.61974440e-10	6.72143036e-08	1.17127082e-06	0.95	3.07827728e-07
58.5	-1.01763203e-09	4.54759489e-07	1.65241671e-05	0.91	3.09599754e-06
59.5	-1.56307209e-10	6.36007172e-08	3.86630485e-06	0.92	3.58530411e-07
60.5	-6.00806861e-10	2.63372194e-07	5.64617215e-07	0.94	1.45080898e-06
61.5	-6.04959878e-10	2.45041951e-07	-1.62883930e-06	0.94	1.21428067e-06
62.5	-6.49554222e-10	2.79301792e-07	1.91126658e-05	0.89	2.08911118e-06
63.5	-4.82850036e-10	1.71382019e-07	2.02470800e-05	0.75	1.67842699e-06
64.5	-1.06653492e-10	4.22914685e-08	1.50553273e-06	0.94	2.03369385e-07
65.5	-8.18714565e-11	3.40516816e-08	1.66550540e-06	0.94	1.76539694e-07
66.5	-9.90389288e-11	4.04518744e-08	1.56394010e-06	0.94	1.96591466e-07
67.5	-9.41472141e-11	3.78395774e-08	8.82049866e-07	0.94	1.80481835e-07
68.5	-8.29145674e-11	3.45290364e-08	5.19960242e-06	0.82	3.44043640e-07
69.5	-1.37956080e-10	5.60239688e-08	1.65024766e-06	0.94	2.65869617e-07
70.5	-1.01440668e-10	4.37751602e-08	9.44754103e-06	0.79	4.90083335e-07
71.5	-8.82187053e-11	3.44490090e-08	2.44945919e-06	0.92	1.89763276e-07
72.5	-1.38052514e-10	5.94292750e-08	4.19292916e-07	0.95	2.87817244e-07
73.5	-4.91176916e-11	2.32864269e-08	1.44437460e-06	0.94	1.39806401e-07
74.5	-6.46953103e-11	2.83325477e-08	2.59377737e-06	0.93	1.66218244e-07
75.5	-7.34309741e-11	3.29461087e-08	4.00460892e-06	0.90	2.45820894e-07
76.5	-3.05657856e-11	2.93068006e-08	1.40723930e-05	0.74	6.32637967e-07
77.5	5.43557600e-11	2.19484499e-08	1.18134495e-05	0.89	5.64382540e-07
78.5	-8.51779066e-11	5.79401798e-08	1.63692915e-05	0.82	8.43951888e-07
79.5	-2.21722606e-10	8.88851417e-08	8.27783879e-06	0.89	6.07167204e-07
80.5	-1.65576278e-10	7.79627572e-08	5.66367756e-06	0.94	4.44114376e-07
81.5	-1.92487027e-10	8.70304770e-08	5.81788594e-06	0.93	5.12896384e-07
82.5	-2.51845067e-10	1.14456368e-07	6.30086163e-06	0.94	6.49515749e-07
83.5	-4.38140196e-10	1.97591643e-07	1.99037756e-05	0.90	1.48395770e-06
84.5	-3.73488547e-10	1.70436208e-07	8.14608828e-06	0.94	9.68131273e-07
85.5	-4.33366783e-10	2.09399580e-07	9.28690005e-06	0.94	1.21724813e-06
86.5	-4.84412766e-10	2.36665683e-07	1.09788284e-05	0.94	1.44126953e-06
87.5	-4.83254202e-10	2.68350608e-07	1.39973835e-05	0.94	1.85920378e-06
88.5	-6.21282703e-10	3.37561898e-07	1.45738166e-05	0.94	2.27765383e-06
89.5	-6.68966301e-10	3.86462205e-07	1.63709915e-05	0.93	2.80715372e-06
90.5	-9.40447671e-10	4.91524881e-07	1.81668436e-05	0.93	3.38519060e-06
91.5	-7.89804624e-10	4.23827993e-07	1.56806295e-05	0.94	2.81369582e-06
92.5	-2.51717440e-10	1.25207391e-07	7.46452895e-06	0.95	7.21226067e-07
93.5	-2.52576412e-10	1.27365730e-07	7.86103295e-06	0.95	7.08295267e-07
94.5	-1.68630601e-10	8.97996451e-08	6.01452925e-06	0.95	5.30470738e-07
95.5	-1.71120327e-10	8.22690427e-08	4.20933726e-06	0.95	4.36420483e-07
96.5	-1.16976002e-10	5.79214134e-08	3.16068207e-06	0.95	3.17857028e-07
97.5	-9.42103907e-10	7.84156346e-07	6.35681772e-05	0.89	9.05302834e-06
98.5	-1.74979936e-10	9.39505851e-08	8.37957920e-06	0.94	6.18586716e-07
99.5	-3.06874683e-10	1.63261897e-07	1.00132945e-05	0.95	9.92576035e-07
100.5	-2.08354284e-10	1.12300476e-07	1.82943275e-06	0.95	6.70876385e-07
101.5	-2.22515562e-10	1.04514427e-07	5.86589870e-06	0.95	5.33557018e-07
102.5	-1.34390246e-09	8.98461854e-07	3.81054263e-05	0.92	7.66619612e-06
103.5	-1.01901721e-09	6.79827099e-07	4.51530159e-05	0.94	5.22679531e-06
104.5	-4.18859821e-10	1.89817197e-07	3.18890523e-06	0.95	9.38122529e-07
105.5	-2.54275033e-10	1.20088332e-07	6.60009868e-06	0.96	5.89125254e-07
106.5	-2.43809593e-10	1.18160635e-07	7.74794070e-06	0.96	5.90449142e-07
107.5	-2.33163874e-10	1.20516330e-07	9.87441885e-06	0.95	6.87291920e-07
108.5	-3.69477413e-10	2.17542411e-07	1.10904940e-05	0.96	1.26819431e-06

109.5	-2.81707873e-10	1.45887138e-07	9.82531461e-06	0.95	7.99552250e-07
110.5	-9.10934796e-11	1.04423228e-07	1.44644224e-05	0.92	1.08652364e-06
111.5	-1.66854605e-10	1.18197160e-07	1.27341149e-05	0.95	8.46551633e-07
112.5	-1.97256040e-10	1.22023811e-07	1.39870362e-05	0.95	8.24895534e-07
113.5	-1.84532308e-10	1.04923564e-07	7.42101884e-06	0.95	6.63927760e-07
114.5	-1.82255068e-10	1.00964734e-07	1.09676338e-05	0.95	5.83301149e-07
115.5	-1.79977830e-10	9.70059057e-08	1.45142487e-05	0.95	5.79507535e-07
116.5	-1.14063699e-10	6.14789756e-08	2.11095772e-05	0.95	3.67271760e-07
117.5	-1.19813939e-09	5.28441463e-07	5.22879409e-05	0.95	2.46827715e-06
118.5	-3.17606335e-10	1.43250820e-07	2.42879319e-05	0.95	6.91404625e-07
119.5	-5.07968379e-10	2.73788903e-07	3.79524397e-05	0.95	1.63559867e-06
120.5	-3.91694650e-09	1.76667070e-06	4.67276673e-05	0.95	8.52689227e-06
121.5	-2.10473407e-08	3.12348452e-05	4.59160841e-03	0.91	3.68717499e-04
122.5	-9.24069369e-10	4.16785440e-07	4.09787537e-05	0.95	2.01162816e-06
123.5	-6.22067015e-10	2.80572523e-07	2.53756139e-05	0.95	1.35419220e-06
124.5	-4.72854326e-10	2.13272731e-07	1.79398692e-05	0.95	1.02936761e-06
125.5	-2.37088928e-10	1.27788104e-07	2.05651276e-05	0.95	7.63398559e-07
126.5	-7.26808556e-10	3.27814376e-07	1.76920985e-05	0.95	1.58220650e-06
127.5	-1.57815999e-10	8.50609426e-08	1.52935833e-05	0.95	5.08149030e-07
128.5	-1.17377545e-10	6.32650980e-08	1.23296767e-05	0.95	3.77941945e-07
129.5	-5.73834119e-11	7.57079693e-08	1.75886126e-05	0.93	7.63296694e-07
130.5	-1.24053248e-09	5.70638506e-07	1.20965081e-04	0.91	4.16222369e-06
131.5	-2.12721218e-10	9.61118248e-08	1.95150657e-05	0.91	6.62435421e-07
132.5	-1.07001857e-10	6.29334120e-08	1.62571838e-05	0.90	5.67873985e-07
133.5	-8.94382834e-10	8.71939234e-07	1.31975911e-04	0.94	7.54203153e-06
134.5	-8.35494200e-11	6.28665121e-08	1.35754292e-05	0.88	7.29144198e-07
135.5	-1.25088026e-10	8.54845405e-08	3.77824430e-05	0.90	8.81264590e-07
136.5	-9.79967900e-11	7.22954986e-08	2.10731394e-05	0.90	7.68205303e-07
137.5	-1.24013546e-10	7.97949440e-08	2.37165611e-05	0.91	7.11357554e-07
138.5	-7.39876006e-11	5.55570063e-08	2.54832371e-05	0.87	6.99090195e-07
139.5	-9.49205508e-10	4.89958571e-07	4.33705249e-05	0.96	2.54613277e-06
140.5	-5.67937224e-10	3.05432744e-07	4.62582464e-05	0.95	1.88073609e-06
141.5	-2.43621952e-10	1.13736869e-07	3.27628394e-05	0.90	8.95784614e-07
142.5	-1.95955912e-10	1.01825495e-07	3.75119030e-05	0.83	1.18926525e-06
143.5	-2.46624207e-10	1.15175318e-07	4.23845795e-05	0.88	1.00877166e-06
144.5	-1.61278923e-10	8.93582633e-08	4.38438448e-05	0.86	9.81989792e-07
145.5	-2.75726953e-10	1.38512452e-07	4.32208222e-05	0.89	1.19372564e-06
146.5	-2.43757781e-10	1.36559581e-07	5.45324615e-05	0.89	1.27366067e-06
147.5	-2.46147842e-10	1.39066818e-07	7.11427892e-05	0.89	1.35250470e-06
148.5	-3.12927956e-10	1.56053330e-07	7.20397030e-05	0.87	1.51332205e-06
149.5	-2.31230729e-10	1.24944106e-07	6.58375866e-05	0.83	1.51364906e-06
150.5	-2.43791216e-10	1.21205065e-07	7.57760769e-05	0.80	1.52268475e-06
151.5	-1.94987017e-10	1.16236962e-07	8.38650446e-05	0.80	1.65675848e-06
152.5	-4.33361801e-10	2.37558655e-07	9.63535070e-05	0.91	2.01495486e-06
153.5	-1.73871412e-10	1.71988954e-07	1.12191003e-04	0.88	2.21903105e-06
154.5	-1.16988909e-09	6.16487236e-07	1.70987119e-04	0.93	4.36900801e-06
155.5	-2.55020760e-10	2.92214578e-07	1.64242591e-04	0.92	3.20494890e-06
156.5	-4.53027932e-10	2.51428725e-07	1.68458783e-04	0.85	2.85808410e-06
157.5	-1.72784194e-10	1.48582781e-07	1.57486859e-04	0.77	2.79008511e-06
158.5	-2.29772147e-10	1.46877406e-07	1.54423418e-04	0.74	2.69140338e-06
159.5	-9.39400590e-11	1.10698536e-07	1.54968996e-04	0.73	2.59598688e-06
160.5	-8.39077851e-11	1.26638098e-07	1.71073746e-04	0.77	2.80522066e-06
161.5	-1.98721268e-10	1.37610016e-07	2.05647262e-04	0.65	3.39322701e-06

162.5	-4.73652596e-10	2.82618134e-07	2.23170447e-04	0.82	3.76275218e-06
163.5	-1.55191039e-10	2.30331717e-07	2.39080251e-04	0.83	4.07902394e-06
164.5	-4.04165128e-10	3.37772150e-07	2.81318936e-04	0.86	4.56771102e-06
165.5	-7.73823055e-12	2.97227900e-07	4.63250839e-04	0.76	7.93202201e-06
166.5	4.07530120e-11	8.57496540e-08	3.29404588e-04	0.51	5.05815432e-06
167.5	-2.04674881e-10	3.39319234e-07	3.67674446e-04	0.81	6.73876290e-06
168.5	-4.43360209e-10	2.79935936e-07	4.04891772e-04	0.66	6.38829474e-06
169.5	1.21153174e-10	2.01744392e-07	5.46199225e-04	0.64	8.70736220e-06
170.5	-5.85190609e-10	4.32779772e-07	6.13206686e-04	0.68	1.01094842e-05
171.5	-5.06522331e-10	4.47020613e-07	6.17992427e-04	0.70	1.06043009e-05
172.5	-3.24768827e-10	3.72615949e-07	6.98235220e-04	0.60	1.23238287e-05
173.5	5.76888817e-11	2.79814116e-07	6.97522794e-04	0.61	1.18627791e-05
174.5	-1.17218795e-10	3.92089797e-07	8.58418577e-04	0.61	1.50705494e-05
175.5	-1.37607193e-10	5.06896902e-07	1.04781557e-03	0.60	1.97468460e-05
176.5	-8.96657609e-10	6.78269058e-07	1.12910891e-03	0.59	2.01888857e-05
177.5	1.32627992e-09	1.79727927e-07	1.42010797e-03	0.47	2.90878237e-05
178.5	1.98167580e-09	8.00937083e-08	1.59925973e-03	0.48	3.18302836e-05
179.5	1.18969584e-09	3.52847586e-07	1.62399680e-03	0.54	3.13644235e-05
180.5	-1.61188575e-09	1.46962414e-06	2.01940644e-03	0.62	4.36405768e-05
181.5	-3.61654690e-09	2.50708549e-06	2.31968020e-03	0.66	5.98817371e-05
182.5	1.44002194e-10	8.58952566e-07	2.34991118e-03	0.46	5.34544458e-05
183.5	-5.43430484e-10	9.53841592e-07	2.52448745e-03	0.45	5.15037308e-05
184.5	-1.30322879e-09	9.76484389e-07	2.20300301e-03	0.47	3.95649715e-05
185.5	-1.62506964e-09	1.13882183e-06	2.50603519e-03	0.44	4.83075423e-05
186.5	-1.89245396e-09	1.37388136e-06	2.88406355e-03	0.44	5.91202561e-05
187.5	6.84720021e-10	6.10050906e-07	3.29718092e-03	0.35	6.56653209e-05
188.5	1.53237630e-09	8.38490308e-07	3.18211645e-03	0.46	7.35219971e-05
189.5	7.23049173e-09	-4.24163156e-07	2.42571457e-03	0.51	6.85476734e-05

412

413

414

415

416

417

Table A2: The Aero-SPAM model describing the photon flux (I , $\text{m}^{-2}\cdot\text{s}^{-1}\cdot\text{nm}^{-1}$) in 37 specified spectral channels depending on the daily $F_{10.7}$ index, $I = P_1 \cdot F_{10.7}^2 + P_2 \cdot F_{10.7} + P_3$. P_1 , P_2 and P_3 are the regression coefficients for the 37 EUV spectral intervals (λ) including 17 lines and 20 bands. R is a correlation coefficient between $F_{10.7}$ and photon flux. RMSE is the root-mean-square error for the measured and simulated I values.

$N\lambda$	$\lambda_{\text{min}}, \text{nm}$	$\lambda_{\text{max}}, \text{nm}$	P_1	P_2	P_3	R	RMSE
1	5	10	-7.22814128e+06	4.34844365e+09	-1.63154083e+11	0.96	2.49833157e+10
2	10	15	-1.72793713e+08	1.06538527e+11	-2.83695953e+12	0.96	6.38391466e+11
3	15	20	-1.79873111e+09	1.05716281e+12	-2.74337230e+13	0.96	6.09484906e+12
4	20	25	-1.67014302e+09	9.88384185e+11	-3.90160466e+13	0.96	5.65031654e+12
5	25.6		-2.42136993e+08	1.44676220e+11	-7.27167455e+12	0.96	8.22340432e+11
6	28.4		-2.15749026e+08	1.47186233e+11	-5.25550336e+12	0.92	1.36257538e+12
7	25	30	-8.49047253e+08	4.39836923e+11	-1.07767192e+13	0.96	2.37564549e+12
8	30.3		-1.05374887e+09	6.15749059e+11	2.21870265e+13	0.94	4.36129879e+12
9	30	35	-5.78821182e+08	4.09300016e+11	-7.39277758e+12	0.93	3.67860958e+12
10	36.8		-3.67641064e+08	2.23500665e+11	-3.44107714e+12	0.93	1.76712865e+12
11	35	40	-5.27393084e+08	2.60815376e+11	-4.81963679e+12	0.94	1.61468490e+12
12	40	45	-1.76485806e+08	9.43602417e+10	1.20746026e+12	0.95	5.78446944e+11
13	46.5		-9.16428947e+06	1.10576870e+10	3.46127070e+12	0.84	1.99324850e+11
14	45	50	-3.28417068e+08	1.54464379e+11	2.70338559e+11	0.96	7.65976697e+11
15	50	55	-4.35029980e+08	1.94267789e+11	-9.12633707e+11	0.96	9.17807984e+11
16	55.4		-7.45540942e+07	2.70143268e+10	6.20498828e+12	0.60	4.21493552e+11
17	58.4		-2.67242090e+08	1.26513904e+11	5.22846617e+12	0.91	9.60988214e+11
18	55	60	-1.11331394e+08	4.91943896e+10	2.59480808e+12	0.94	2.86378660e+11

19	60.9		-1.75317009e+08	7.84311521e+10	2.56019089e+11	0.94	4.50958343e+11
20	62.9		-1.95380036e+08	8.57116193e+10	6.10932407e+12	0.89	6.88675932e+11
21	60	65	-3.18739604e+08	1.31380748e+11	7.10288562e+12	0.90	8.93006924e+11
22	65	70	-1.54464890e+08	6.57942854e+10	3.90335230e+12	0.93	3.82370215e+11
23	70.3		-3.92892316e+07	1.62255869e+10	3.31133072e+12	0.78	1.84543928e+11
24	70	75	-1.17284653e+08	5.16415922e+10	2.62008424e+12	0.94	2.82746960e+11
25	76.5		-2.80655392e+07	1.48549365e+10	5.22726113e+12	0.72	2.63413854e+11
26	77.0		-1.42682444e+07	1.64116032e+10	4.19804672e+12	0.88	2.42046487e+11
27	78.9		-5.13752841e+07	2.67845754e+10	6.25669926e+12	0.81	3.56475663e+11
28	75	80	-1.09163517e+08	4.63578518e+10	4.91238247e+12	0.89	3.39676578e+11
29	80	85	-5.71385988e+08	2.65288858e+11	1.93295978e+13	0.94	1.62478581e+12
30	85	90	-1.26716263e+09	6.53242857e+11	2.77927431e+13	0.94	4.18839876e+12
31	90	95	-1.14503862e+09	5.87977430e+11	2.50221903e+13	0.95	3.62200988e+12
32	97.8		-4.60750790e+08	3.84479195e+11	3.11115764e+13	0.90	4.64901797e+12
33	95	100	-3.84402107e+08	1.97008185e+11	1.26370475e+13	0.95	1.14344491e+12
34	102.6		-7.45028477e+08	4.75205812e+11	1.89621526e+13	0.93	4.08952635e+12
35	103.2		-6.18608147e+08	3.73585739e+11	2.24459796e+13	0.94	2.81357100e+12
36	100	105	-4.16550795e+08	2.04940624e+11	5.82827246e+12	0.96	1.07697392e+12
37	121.6		-2.81408845e+10	2.25475006e+13	2.62203706e+15	0.92	2.35540620e+14

418

419 **Data Availability Statement**

420 The authors are grateful for the provided data used in this work. F10.7 solar activity index is
421 available at OMNIweb Plus database (<https://omniweb.gsfc.nasa.gov/ow.html>). TIMED SEE
422 data are available at LASP Interactive Solar Irradiance Data Center
423 (<https://lasp.colorado.edu/home/see/data/>). F10.7 forecast is provided by IZMIRAN Space
424 Weather prediction Center (<http://spaceweather.izmiran.ru/eng/forecasts.html>).

425 The SPAM model scripts are available on Zenodo (<https://zenodo.org/record/6985548>,
426 DOI:10.5281/zenodo.6985548).

427

428 **References**

429 Banks, P.M., & Kockarts, G., 2013. *Aeronomy*. Elsevier.
430 Brasseur, G.P., & Solomon, S., 2005. *Aeronomy of the Middle Atmosphere: Chemistry and
431 Physics of the Stratosphere and Mesosphere*. Springer Dordrecht. doi:10.1007/1-4020-3824-0.

- 432 Bruevich, E., & Yakunina, G., 2019. Flux variations in lines of solar euv radiation beyond
433 flares in cycle 24. *Geomagnetism and Aeronomy* 59, 155–161.
434 doi:10.1134/S0016793219020038.
- 435 Byram, E., Chubb, T., & Friedman, H., 1956. The solar X-ray spectrum and the density of
436 the upper atmosphere. *Journal of Geophysical Research* 61,251–263.
437 doi:10.1029/JZ061i002p00251.
- 438 Cervera, M.A., Harris, T.J., Holdsworth, D.A., & Netherway, D.J., 2021. Ionospheric
439 effects on HF radio wave propagation. *Ionosphere Dynamics and Applications*, 439–492.
440 doi:10.1002/9781119815617.ch19.
- 441 Chamberlin, P.C., Eparvier, F.G., Knoer, V., Leise, H., Pankratz, A., Snow, M.,
442 Templeman, B., Thiemann, E.M.B., Woodraska, D.L., & Woods, T.N., 2020. The flare
443 irradiance spectral model-version 2 (FISM2). *Space Weather* 18, e2020SW002588.
444 doi:10.1029/2020SW002588.
- 445 Chamberlin, P.C., Woods, T.N., & Eparvier, F.G., 2007. Flare irradiance spectral model
446 (FISM): Daily component algorithms and results. *Space Weather* 5(7).
447 doi:10.1029/2007SW000316.
- 448 Chamberlin, P.C., Woods, T.N., & Eparvier, F.G., 2008. Flare irradiance spectral model
449 (FISM): Flare component algorithms and results. *Space Weather* 6(5).
450 doi:10.1029/2007SW000372.
- 451 Chapman, S., 1931. The absorption and dissociative or ionizing effect of monochromatic
452 radiation in an atmosphere on a rotating earth. *Proceedings of the Physical Society* (1926-1948)
453 43, 26. doi:10.1088/0959- 5309/43/1/305.

- 454 Del Zanna, G., & Mason, H.E., 2018. Solar UV and X-ray spectral diagnostics. *Living*
455 *Reviews in Solar Physics* 15, 1–278. doi:10.1007/s41116-018-0015-3.
- 456 Didkovsky, L., Judge, D., Wieman, S., Woods, T., & Jones, A., 2009. EUV
457 spectrophotometer (ESP) in extreme ultraviolet variability experiment (EVE): algorithms
458 and calibrations, in: *The solar dynamics observatory*. Springer, pp. 179–205.
459 doi:10.1007/s11207-009-9485-8.
- 460 Dudok de Wit, T., 2022. Detecting undocumented trends in solar irradiance observations.
461 *Journal of Space Weather and Space Climate* 12, 10. doi:10.1051/swsc/2021041.
- 462 Fuller-Rowell, T., Solomon, S., Roble, R., & Viereck, R., 2004. Impact of solar EUV, XUV,
463 and X-ray variations on earth's atmosphere. *Geophysical monograph* 141, 341–354.
464 doi:10.1029/141GM23.
- 465 Gaidash, S., Belov, A., Abunina, M., & Abunin, A., 2017. Space weather forecasting at
466 IZMIRAN. *Geomagnetism and Aeronomy* 57, 869–876. doi:10.1134/S0016793217070088.
- 467 Gao, H., Li, G., Li, Y., Yang, Z., & Wu, X., 2006. Ionospheric effect of HF surface wave
468 over-the-horizon radar. *Radio science* 41, 1–10. doi:10.1029/2005RS003323.
- 469 Girazian, Z., & Withers, P., 2015. An empirical model of the extreme ultraviolet solar
470 spectrum as a function of F10.7. *Journal of Geophysical Research: Space Physics* 120,
471 6779–6794. doi:10.1002/2015JA021436.
- 472 Gray, L.J., Beer, J., Geller, M., Haigh, J.D., Lockwood, M., Matthes, K., Cubasch, U.,
473 Fleitmann, D., Harrison, G., Hood, L., Luterbacher J., Meehl G. A., Shindell D., van Geel
474 B., & White W., 2010. Solar influences on climate. *Reviews of Geophysics* 48.
475 doi:10.1029/2009RG000282.

- 476 Henney, C., Toussaint, W., White, S., & Arge, C., 2012. Forecasting F10.7 with solar
477 magnetic flux transport modeling. *Space Weather* 10. doi:10.1029/2011SW000748.
- 478 Huang, C., Liu, D.D., & Wang, J.S., 2009. Forecast daily indices of solar activity, f10. 7,
479 using support vector regression method. *Research in Astronomy and Astrophysics* 9, 694.
480 doi:10.1088/1674-4527/9/6/008.
- 481 Kaufmann, P., & Paes de Barros, M., 1969. Some relationships between solar X-ray bursts and
482 SPA's produced on VLF propagation in the lower ionosphere. *Solar Physics* 9, 478–486.
483 doi:10.1007/BF02391673.
- 484 Klimov, P., Sigaeva, K., & Sharakin, S., 2021. Flight calibration of the photodetector in the
485 TUS detector. *Instruments and Experimental Techniques* 64, 450–455.
486 doi:10.1134/S0020441221030192.
- 487 Kretzschmar, M., Dudok de Wit, T., Lilensten, J., Hochedez, J.F., Abouadarham, J.,
488 Amblard, P.O., Auchère, F., & Moussaoui, S., 2009. Solar EUV/FUV irradiance variations:
489 analysis and observational strategy. *Acta Geophysica* 57, 42–51. doi:10.2478/s11600-008-
490 0066-2.
- 491 Lanchester, B., Rees, M., Lummerzheim, D., Otto, A., Sedgemore-Schulthess, K., Zhu, H.,
492 & McCrea, I., 2001. Ohmic heating as evidence for strong field-aligned currents in
493 filamentary aurora. *Journal of Geophysical Research: Space Physics* 106, 1785–1794.
494 doi:10.1029/1999JA000292.
- 495 LASP Interactive Solar Irradiance Data Center, a. FISM-P Earth Solar Spectral
496 Irradiance, Time Series. https://lasp.colorado.edu/lisird/data/fism_p_ssi_earth/. Online;
497 accessed 4 August 2022.

- 498 LASP Interactive Solar Irradiance Data Center, b. TIMED SEE Database.
499 <http://lasp.colorado.edu/home/see/data>. Online; accessed 4 August 2022.
- 500 LASP Interactive Solar Irradiance Data Center, c. TIMED SEE Level 3A Data
501 Products description.
502 http://lasp.colorado.edu/data/timed_see/level3a/README_SEE_L3A_012.TXT. Online;
503 accessed 4 August 2022.
- 504 LASP Interactive Solar Irradiance Data Center, d. TIMED SEE Version 12 Data Product
505 Release Notes. http://lasp.colorado.edu/data/timed_see/SEE_v12_releasenotes.txt. Online;
506 accessed 4 August 2022.
- 507 Lean, J., 1987. Solar ultraviolet irradiance variations: A review. *Journal of Geophysical*
508 *Research: Atmospheres* 92, 839–868. doi:10.1029/JD092iD01p00839.
- 509 Lean, J., 1990. A comparison of models of the sun’s extreme ultraviolet irradiance
510 variations. *Journal of Geophysical Research: Space Physics* 95, 11933–11944. doi:10.1029/
511 JA095iA08p11933.
- 512 Lean, J., White, O., Livingston, W., & Picone, J., 2001. Variability of a composite
513 chromospheric irradiance index during the 11-year activity cycle and over longer time periods.
514 *Journal of Geophysical Research: Space Physics* 106, 10645–10658.
515 doi:10.1029/2000JA000340.
- 516 Lean, J., Woods, T., Eparvier, F., Meier, R., Strickland, D., Correira, J., & Evans, J.,
517 2011. Solar extreme ultraviolet irradiance: Present, past, and future. *Journal of*
518 *Geophysical Research: Space Physics* 116. doi:10.1029/2010JA015901.

- 519 Lei, L., Zhong, Q., Wang, J., Shi, L., & Liu, S., 2019. The mid-term forecast method of f10.
520 7 based on extreme ultraviolet images. *Advances in Astronomy 2019*.
521 doi:10.1155/2019/5604092.
- 522 Lilensten, J., Dudok de Wit, T., Kretzschmar, M., Amblard, P.O., Moussaoui, S.,
523 Abouadarham, J., & Auchère, F., 2008. Review on the solar spectral variability in the EUV for
524 space weather purposes, in: *Annales Geophysicae, Copernicus GmbH*. pp. 269–279.
525 doi:10.1002/2017SW001725.
- 526 Mauceri, S., Richard, E., Pilewskie, P., Harber, D., Coddington, O., Béland, S.,
527 Chambliss, M., & Carson, S., 2020. Degradation correction of TSIS SIM. *Solar Physics 295*,
528 1–21. doi:10.1007/s11207-020-01707-y.
- 529 Nikolaeva, V., Gordeev, E., Nikolaev, A., Rogov, D., & Troshichev, O., 2022a. Auroral
530 ionosphere model with PC index as an input. *Atmosphere 13*, 402.
531 doi:10.3390/atmos13030402.
- 532 Nikolaeva, V., Gordeev, E., Rogov, D., & Nikolaev, A., 2021a. Auroral ionosphere model
533 (AIM-E) adjustment for the regular E layer. *Solar-Terrestrial Physics 7*, 41–46.
534 doi:10.12737/szf-71202106.
- 535 Nikolaeva, V., Gordeev, E., Rogov, D., & Novikov, S., 2022b. Calibration of empirical
536 EUV spectra for the regular e-region modeling. *Bulletin of the Russian Academy of*
537 *Sciences: Physics 86*, 329–334. doi:10.3103/S1062873822030194.
- 538 Nikolaeva, V., Gordeev, E., Sergienko, T., Makarova, L., & Kotikov, A., 2021b. AIM-E: E-
539 region auroral ionosphere model. *Atmosphere 12*, 748. doi:10.3390/atmos12060748.
- 540 Nusinov, A., Antonova, L., Kazachevskaya, T., Katyushina, V., & Svidsky, P., 2000. 11-
541 year solar cycle extreme ultraviolet and soft X-ray variations according to the ionospheric e-

- 542 region data and results of direct measurements. *Advances in Space Research* 25, 73–78.
543 doi:10.1016/S0273- 1177(99)00900-X.
- 544 Nusinov, A.A., Kazachevskaya, T.V., & Katyushina, V.V., 2021. Solar extreme and far
545 ultraviolet radiation modeling for aeronomic calculations. *RemoteSensing* 13, 1454.
546 doi:10.3390/rs13081454.
- 547 Ohshio, M., Maeda, R., & Sakagami, H., 1966. Height distribution of local photoionization
548 efficiency. *J. Radio Res. Lab* 13, 245.
- 549 Pacini, A.A., & Raulin, J.P., 2006. Solar X-ray flares and ionospheric sudden phase
550 anomalies relationship: A solar cycle phase dependence. *Journal of Geophysical Research:*
551 *Space Physics* 111. doi:10.1029/2006JA011613.
- 552 Picone, J., Hedin, A., Drob, D.P., & Aikin, A., 2002. NRLMSISE-00 empirical model of the
553 atmosphere: Statistical comparisons and scientific issues. *Journal of Geophysical Research:*
554 *Space Physics* 107, SIA–15. doi:10.1029/2002JA009430.
- 555 Qian, L., & Solomon, S.C., 2012. Thermospheric density: An overview of temporal and
556 spatial variations. *Space science reviews* 168, 147–173. doi:10.1007/s11214-011-9810-z.
- 557 Richards, P., Fennelly, J., & Torr, D., 1994. EUVAC: A solar EUV flux model for
558 aeronomic calculations. *Journal of Geophysical Research: Space Physics* 99, 8981–8992.
559 doi:10.1029 / 94JA00518.
- 560 Richards, P.G., Woods, T.N., & Peterson, W.K., 2006. HEUVAC: A new high resolution
561 solar EUV proxy model. *Advances in Space Research* 37, 315–322.
562 doi:10.1016/j.asr.2005.06.031.
- 563 Rozanov, E., Egorova, T., Schmutz, W., & Peter, T., 2006. Simulation of the stratospheric
564 ozone and temperature response to the solar irradiance variability during sun rotation cycle.

565 *Journal of Atmospheric and Solar-Terrestrial Physics* 68, 2203–2213.
566 doi:10.1016/j.jastp.2006.09.004.

567 Schmidtke, G., 2015. Extreme ultraviolet spectral irradiance measurements since 1946. *History*
568 *of Geo-and Space Sciences* 6, 3–22. doi:10.5194/hgss-6-3-2015.

569 Schunk, R., & Nagy, A., 1980. Ionospheres of the terrestrial planets. *Reviews of Geophysics*
570 18, 813–852. doi:10.1029/RG018i004p00813.

571 Smith III, F., & Smith, C., 1972. Numerical evaluation of Chapman’s grazing incidence
572 integral $ch(x, \chi)$. *Journal of Geophysical Research* 77, 3592– 3597.
573 doi:10.1029/JA077i019p03592.

574 Snow, M., McClintock, W., & Woods, T., 2010. Solar spectral irradiance variability in the
575 ultraviolet from SORCE and UARS SOLSTICE. *Advances in Space Research* 46, 296–302.
576 doi:10.1016/j.asr.2010.03.027.

577 Space Weather Prediction Center (IZMIRAN). Review and forecast of solar and
578 geomagnetic activity (IZMIRAN). <http://spaceweather.izmiran.ru/eng/forecasts.html>.
579 Online; accessed 4 August 2022.

580 Space Weather Prediction Center of National Oceanic and Atmospheric Administration, a.
581 NOAA 20-years Sunspot Number and 10.7 cm Radio Flux and Geomagnetic Indices
582 Prediction. <https://www.swpc.noaa.gov/products/usaf-45-day-ap-and-f107cm-flux-forecast>.
583 Online; accessed 4 August 2022.

584 Space Weather Prediction Center of National Oceanic and Atmospheric Administration, b.
585 NOAA 27-Day Outlook of 10.7 cm Radio Flux and Geomagnetic Indices.
586 [https://www.swpc.noaa.gov/products/27-day-outlook-107-cm-radio-flux-and-geomagnetic-](https://www.swpc.noaa.gov/products/27-day-outlook-107-cm-radio-flux-and-geomagnetic-indices)
587 [indices](https://www.swpc.noaa.gov/products/27-day-outlook-107-cm-radio-flux-and-geomagnetic-indices). Online; accessed 4 August 2022.

588 Space Weather Prediction Center of National Oceanic and Atmospheric Administration, c.
589 NOAA 45-Day Outlook of 10.7 cm Radio Flux and Geomagnetic Indices.
590 <https://www.swpc.noaa.gov/products/usaf-45-day-ap-and-f107cm-flux-forecast>. Online;
591 accessed 4 August 2022.

592 SPDF Goddard Space Flight Center. OMNIWeb Database.
593 <https://omniweb.gsfc.nasa.gov/ow.html>. Online; accessed 4 August 2022.

594 Svalgaard, L., 2013. Solar activity – past, present, future. *Journal of Space Weather and Space*
595 *Climate* 3, A24. doi:10.1051/swsc/2013046/.

596 Tapping, K., 2013. The 10.7 cm solar radio flux (f10.7). *Space weather* 11, 394–406.
597 doi:10.1002/swe.20064.

598 Tobiska, W., 1996. Current status of solar EUV measurements and modeling. *Advances in*
599 *Space Research* 18, 3–10. doi:10.1016/0273-1177(95)00827-2.

600 Tobiska, W.K., & Eparvier, F., 1998. EUV97: Improvements to EUV irradiance modeling
601 in the soft X-rays and FUV. *Solar Physics* 177, 147–159. doi:10.1023/A:1004931416167.

602 Torr, D., & Torr, M.R., 1979. Chemistry of the thermosphere and ionosphere. *Journal of*
603 *Atmospheric and Terrestrial Physics* 41, 797–839. doi:10.1016/0021-9169(79)90126-0.

604 Vaishnav, R., Jacobi, C., Berdermann, J., Schmölter, E., & Codrescu, M., 2018.
605 Ionospheric response to solar euv variations: Preliminary results. *Advances in Radio Science*
606 *16*, 157–165. doi:10.5194/ars-16-157-2018.

607 Verronen, P., Andersson, M., Marsh, D., Kovács, T., & Plane, J., 2016. WACCM-D —
608 Whole Atmosphere Community Climate Model with D-region ion chemistry. *Journal of*
609 *Advances in Modeling Earth Systems* 8, 954–975. doi:10.1002/2015MS000592.

- 610 Vourlidas, A., & Bruinsma, S., 2018. EUV irradiance inputs to thermospheric density models:
611 Open issues and path forward. *Space Weather* 16, 5–15. doi:10.1002/2017SW001725.
- 612 Ward W., Seppälä A., Yiğit E., Nakamura T., Stolle C., Laštovička J., Woods T.N., Tomikawa Y.,
613 Lübken F.-J., Solomon S.C., Marsh D.R., Funke B. & Pallamraju D., 2021. Role of the sun and
614 the middle atmosphere/thermosphere/ionosphere in climate (ROSMIC): a retrospective and
615 prospective view. *Progress in Earth and Planetary Science* 8, 1–38. doi:10.1186/s40645-
616 021-00433-8.
- 617 Woodraska, D.L., Woods, T.N., & Eparvier, F.G., 2004. In-flight calibration and
618 performance of the solar extreme ultraviolet experiment (SEE) aboard the timed satellite, in:
619 *Instruments, Science, and Methods for Geospace and Planetary Remote Sensing, SPIE*. pp.
620 36–47. doi:10.1117/12.579034.
- 621 Woods, T.N., 2008. Recent advances in observations and modeling of the solar ultraviolet and
622 X-ray spectral irradiance. *Advances in Space Research* 42, 895–902.
623 doi:10.1016/j.asr.2007.09.026.
- 624 Woods, T.N., Rottman, G.J., Harder, J.W., Lawrence, G.M., McClintock, W.E., Kopp, G.A.,
625 & Pankratz, C., 2000. *Overview of the EOS SORCE mission, in: Earth Observing Systems V,*
626 *SPIE*. pp. 192–203. doi:10.1117/12.494229.
- 627 Zhang, W., Zhao, X., Feng, X., Liu, C., Xiang, N., Li, Z., & Lu, W., 2022. Predicting the
628 daily 10.7-cm solar radio flux using the long short-term memory method. *Universe* 8, 30.
629 doi:10.3390/universe8010030.